

Development and characterization of an omnidirectional photoacoustic point source for calibration of a staring 3D photoacoustic imaging system

Michael Roumeliotis^{1,2}, Pinhas Ephrat^{1,2}, John Patrick¹, Jeffrey J. L. Carson^{1,2,*}

¹Imaging Program, Lawson Health Research Institute, St. Joseph's Health Care, 268 Grosvenor St., London, Ontario, N6A 4V2, Canada

²Department of Medical Biophysics, Schulich School of Medicine and Dentistry, The University of Western Ontario, London, Ontario, N6A 5C1, Canada

*jcarson@lawsonimaging.ca

Abstract: Photoacoustic imaging is a modality which makes use of the contrast provided by optical imaging techniques and the spatial resolution and penetration depth similar to acoustic imaging modalities. We have developed a method for fast 3D photoacoustic imaging using a sparse hemispherical array of transducers. Such a system requires characterization of the transducer's response to an ideal point source in order to accurately reconstruct objects in the imaging volume. First, an attempt was made to design an ideal photoacoustic point source via a combination of liquids which would appropriately scatter and absorb the light such that a spherical distribution was achieved. Methylene blue (MB⁺) was used as the primary optical absorber while Intralipid (IL) was used as the liquid responsible for the optical scatter. A multitude of combinations were tested and the signal uniformity was characterized. The combination of 200 μ M MB⁺ and 0.09% IL was found to produce the most uniform signal over the range of transducers in the hemispherical array. The liquid source was then characterized over a broader range of azimuthal and zenith angles where it was shown the azimuthal consistency was much greater than the stability seen in different zenith elevations. The source was then used in a calibration scan for an imaging volume of 40x40x40 mm³. At 216 points evenly spaced in the imaging volume, parameters were recorded for signal amplitude, width, and time-of-flight. These calibration parameters could then be applied to an iterative reconstruction algorithm in an attempt to more accurately produce images.

©2009 Optical Society of America

OCIS codes: (170.5120) Photoacoustic imaging; (170.3010) Image reconstruction techniques

References and links

1. T. Lu, J. Jiang, Y. Su, R. K. Wang, F. Zhang, and J. Yao, "Photoacoustic imaging: Its current status and future development," in *4th International Conference on Photonics and Imaging in Biology and Medicine*, (SPIE, 2006), **6047**.
2. M. Xu, and L. V. Wang, "Photoacoustic imaging in biomedicine," *Rev. Sci. Instrum.* **77**(4), 041101 (2006).
3. G. J. Diebold, T. Sun, and M. I. Khan, "Photoacoustic monopole radiation in one, two, and three dimensions," *Phys. Rev. Lett.* **67**(24), 3384–3387 (1991).
4. G. Paltauf, J. A. Viator, S. A. Prahl, and S. L. Jacques, "Iterative reconstruction algorithm for optoacoustic imaging," *J. Acoust. Soc. Am.* **112**(4), 1536–1544 (2002).
5. P. Liu, "The P-transform and photoacoustic image reconstruction," *Phys. Med. Biol.* **43**(3), 667–674 (1998).
6. C. G. A. Hoelen, and F. F. M. de Mul, "Image reconstruction for photoacoustic scanning of tissue structures," *Appl. Opt.* **39**(31), 5872–5883 (2000).

7. D. Frauchiger, K. P. Kostli, G. Paltauf, M. Frenz, and H. P. Weber, "Optoacoustic tomography using a two dimensional optical pressure transducer and two different reconstruction algorithms," in *Hybrid and Novel Imaging and New Optical Instrumentation for Biomedical Applications*, (SPIE, 2001), **4434**, pp. 74–80.
 8. M. Xu, and L. V. Wang, "RF-induced thermoacoustic tomography," in *Proceedings of the 2002 IEEE Engineering in Medicine and Biology 24th Annual Conference and the 2002 Fall Meeting of the Biomedical Engineering Society (BMES / EMBS)*, (Institute of Electrical and Electronics Engineers Inc, 2002), pp. 1211–1212.
 9. D. H. Turnbull, and F. S. Foster, "Fabrication and characterization of transducer elements in two-dimensional arrays for medical ultrasound imaging," *IEEE Trans. Ultrason. Ferroelectr. Freq. Control* **39**(4), 464–475 (1992).
 10. X. Yang, and L. V. Wang, "Photoacoustic tomography of a rat cerebral cortex with a ring-based ultrasonic virtual point detector," *J. Biomed. Opt.* **12**(6), 060507 (2007).
 11. C. Li, and L. V. Wang, "High-numerical-aperture-based virtual point detectors for photoacoustic tomography," *Appl. Phys. Lett.* **93**(3), 033902 (2008).
 12. R. A. Kruger, W. L. Kiser, Jr., D. R. Reinecke, and G. A. Kruger, "Thermoacoustic computed tomography using a conventional linear transducer array," *Med. Phys.* **30**(5), 856–860 (2003).
 13. P. Ephrat, and J. J. L. Carson, "Measurement of photoacoustic detector sensitivity distribution by robotic source placement," in *9th Conference on Photons Plus Ultrasound: Imaging and Sensing 2008*, (SPIE, 2008), **6856**.
 14. F. van der Have, B. Vastenhouw, M. Rentmeester, and F. J. Beekman, "System calibration and statistical image reconstruction for ultra-high resolution stationary pinhole SPECT," *IEEE Trans. Med. Imaging* **27**(7), 960–971 (2008).
 15. Y. Pawitan, S. Kohlmyer, T. Lewellen, and F. O'Sullivan, "PET system calibration and attenuation correction," in *Part 1 (of 3)*, (IEEE, 1996), pp. 1300–1304.
 16. M. Roumeliotis, P. Ephrat, and J. J. L. Carson, "Development of an omni-directional photoacoustic source for the characterization of a hemispherical sparse detector array," in *Photons Plus Ultrasound: Imaging and Sensing 2009: The Tenth Conference on Biomedical Thermoacoustics, Optoacoustics and Acousto-optics* (SPIE 2009) **7177**, 71772F.
 17. P. Ephrat, M. Roumeliotis, F. S. Prato, and J. J. L. Carson, "Four-dimensional photoacoustic imaging of moving targets," *Opt. Express* **16**(26), 21570–21581 (2008).
-

1. Introduction

1.1 Background

Photoacoustic imaging (PAI) is a hybrid modality capable of providing contrast similar to that of direct optical imaging techniques but with increased penetration depth in turbid media by encoding the optical information as acoustic waves [1,2]. The technique utilizes a pulsed laser to diffusely illuminate optically absorbing objects in the turbid medium. For example, in biological systems, the absorbing objects may include blood vessels and areas of neovasculature embedded within the surrounding tissue (i.e. the turbid medium). Provided the laser pulse is sufficiently brief, thermal confinement criteria are met and cause the optically absorbing objects to most efficiently emit the absorbed optical energy as a transient bipolar pressure wave [3]. Information related to the location, size, shape, and optical properties of the absorbing objects is present in the pressure waves [4]. The pressure signals acquired over a number of transducers can be processed by a reconstruction algorithm such that images of the optically absorbing objects can be produced [5–8].

There are a number of challenges linked to accurate image reconstruction of objects. Features of the pressure signals vary depending on the position and physical dimensions of the object [3] as well as the optical absorption characteristics. However, these same features of the pressure signals are also affected by the frequency response and angular acceptance of the ultrasound transducers. Furthermore, due to the interaction of propagating pressure waves with ultrasound transducers of finite dimension, the resultant pressure signals can be broadened and arrive at earlier or later times. Therefore, without detailed information of the system response, all algorithms will reconstruct images of objects that have misregistration artifacts and errors in the size, shape and contrast of the objects.

Characterization of photoacoustic imaging system response has been estimated through several approaches. Most relevant to photoacoustic system calibration are techniques to calibrate conventional ultrasound imaging systems because the angular acceptance of ultrasound transducers is inherent to both imaging modalities. This includes a strategy developed by Foster et. al which characterized the signal produced by a transmitting element

at varying angles off the acoustic transmission axis [9]. Wang et al. [10,11] have implemented ring-shaped ultrasonic transducers which act as virtual point detectors. These virtual point detectors can be used to detect photoacoustic signals in the same way as a real point detector. Therefore, uniform sensitivity to photoacoustic signals throughout the imaging field of view can be assumed during image reconstruction. Kruger et al. [12] have measured the system response by constructing a point source by pulsed illumination of a spot-coated 0.1 mm polyethylene fiber. As the source was translated through the imaging volume, the axial response of the system was measured. In a similar strategy, our lab [13] implemented the use of a point source created by pulsed illumination down an optical fiber to an absorbing tip to characterize the response of a detector array. By translating the source incrementally in the three coordinate directions the response of the array was characterized throughout the entire imaging volume. System response was mapped for each voxel-transducer pair which could later be incorporated into the reconstruction algorithm. Other imaging modalities, including SPECT and PET, have been characterized using similar techniques to obtain the system response [14,15].

1.2 Objective

We have previously reported on a method to fabricate a point source at the tip of an optical fiber [13,16]. Limited success was achieved, leaving opportunity for an improved point source to more accurately characterize the system response. From our earlier results, it appeared as though physical imperfections due to manual construction of the fiber tip caused significant azimuthal signal non-uniformity. As well, predictable, but highly directional emission characteristics were observed in the zenith direction. For a transducer array, that has significant coverage over a large solid angle (e.g. hemispherical array described in [17]), calibration of the system response required that we develop a point source with omnidirectional emission character.

1.3 Approach

Our approach was to construct a fiber optic PA point source where the coated tip was replaced with a liquid medium having optically absorbing and scattering properties. As light is directed into an optically absorbing liquid, the shape of the beam is maintained in a directional path as no scattering component is present. The photons are then absorbed along the directional path which subsequently produces a directional acoustic wave. If a scattering component is then added to the absorbing liquid, the distribution of light in the medium begins to result in a spherical-like shape. When the scattering component becomes too large, a region of high back-scatter is produced near the photon injection site causing the absorption of the photons primarily to occur in a directional pattern at the surface of the liquid. Therefore, it was our goal to develop a liquid with an appropriate balance of both scattering and absorption components which would produce a photoacoustic point source. Ideally, the point source would emit a uniform acoustic wave in both the azimuthal and zenith orientations. The source could later be used to characterize response parameters for signal amplitude, time-of-flight, and width.

2. Methods

2.1 Photoacoustic imaging system

A schematic of the photoacoustic system is shown in Fig. 1(a). The imaging system utilized 15 ultrasound transducers (model V304, 1" Ø, 2.25 MHz with fractional bandwidth of 65%, *Panametrics-NDT*, Waltham, Massachusetts) in a staring hemispherical arrangement. Transducers were mounted on 5 custom-built frame columns, each supporting 3 transducers at zenith angles of 22.5°, 45°, and 67.5°. The design of the frames ensured that the directional sensitivity of all 15 transducer overlapped in a imaging volume of approximately 25x25x25

mm³ near the geometric center of the array. The 5 columns were spread azimuthally by 72° to provide uniform coverage over 360°. The container surrounding the transducers was filled with water to provide an acoustic coupling medium. Laser illumination (“Surelite OPO Plus”, OPO-coupled Nd:YAG, *Continuum*, Santa Clara, California) was directed to a bifurcated fiber (400 μm diameter) such that half the light was directed to a photodiode (to measure pulse-to-pulse variation) and the other half to an optical fiber immersed in the liquid, where the light could be scattered and absorbed. Prior to acquiring acoustic signals, the fiber optic was soaked in the liquid solution for 20 minutes to allow any staining of the fiber to be consistent through experimental iterations. The pulse duration was 6 ns at a repetition rate of 10 Hz with a maximum output of approximately 100 mJ/pulse. All experiments were performed at 675 nm. Each transducer element was electrically connected to a dedicated channel on a preamplifier card (custom built). The analog signals were acquired in parallel, converted to digital signals, and sent to a personal computer for analysis. The data acquisition system was custom built and sampled with 14-bit resolution at a frequency of 50 MHz. Figure 1(a) and Fig. 1(b) illustrate the systems used to characterize the PA point source as well as a representative time trace shown in Fig. 1(c) indicating the metrics used to fully describe wave parameters.

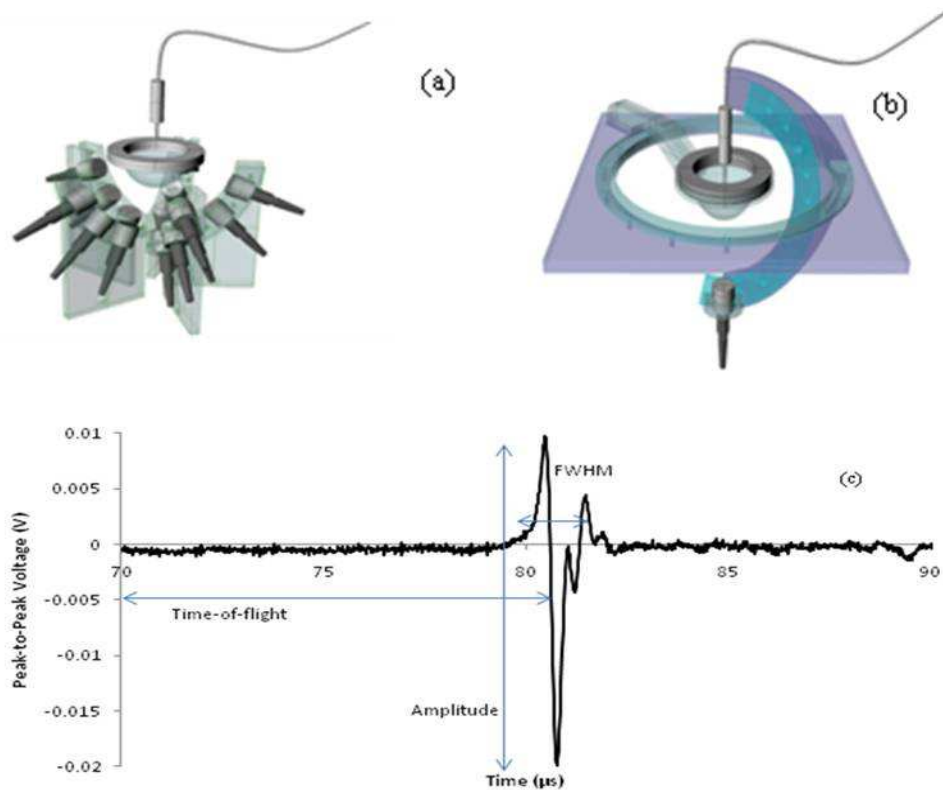


Fig. 1. (a). Isometric view of the hemispherical PA imaging array illustrating the transducer arrangement, placement of the liquid reservoir, and the optical fiber PA source. (b). Isometric view of the system for detailed PA source characterization illustrating one transducer, the transducer arm, the liquid reservoir and the optical fiber. The transducer arm was capable of rotation in 15° increments in the zenith direction and 22.5° increments in the azimuthal direction. (c). Example of raw data acquired on a single acoustic transducer. Signal time-of-flight, amplitude, and FWHM are labeled.

2.2 Source uniformity characterization

The fiber optic cable was mounted to the stage of a *xyz*-scanning gantry and translated to a position where the fiber tip was equidistant from each of the 15 transducers. The fiber tip was immersed entirely in a homogeneous mixture of water, methylene blue, and Intralipid (MB⁺/IL) held within a reservoir at the geometric center of the array as shown in Fig. 1(a). The container was constructed from a supporting ring from which a bag formed from standard kitchen wrap was hung. Methylene blue was added to the reservoir from a 1 mM stock solution. Four different reservoir solutions were tested at methylene blue concentrations of 50, 100, 150, and 200 μM . A separate auxiliary solution of MB⁺/IL was made for each of the corresponding reservoir concentrations. As the auxiliary solution was added to the reservoir solution, the concentration of methylene blue was maintained while the scatter percentage was increased by 0.01%. The reservoir Intralipid concentration was systematically increased from 0 to 0.11% in 0.01% increments. At each condition, the PA signal was sampled for five laser pulses and averaged. The peak-to-peak distance representative of the PA signal amplitude recorded at each transducer was extracted from each averaged time series. The experiment was performed 3 times, each time with fresh solutions.

2.3 Source directionality characterization

Using a separate system for calibration, the directionality of the emission from the liquid PA source was measured with a single transducer at locations equidistant to the PA source in the azimuthal and zenith directions (Fig. 1(b)). In a manner similar to the experiments with the array, the fiber tip was immersed in a MB⁺/IL solution (200 μM MB⁺ and 0.09% Intralipid). At this solution concentration, the absorption and scattering coefficient were approximately 37 cm^{-1} and 4 cm^{-1} , respectively. The arm holding the transducer had the capability to rotate in 15° increments in the zenith direction and 22.5° increments in the azimuthal direction. With the fiber stationary at a position equidistant from all possible transducer locations, the single transducer was rotated every 45° in the azimuth and 15°, 45°, and 75° in the zenith. At each transducer position, the peak-to-peak value of the PA signal was obtained exactly as described above for the array experiment. The experiment was repeated 3 times, each time with fresh solutions.

2.4 System calibration scan

Using a MB⁺/IL solution of identical composition to the solution used for the source directionality characterization experiments, a calibration scan was performed using the liquid PA point source. The fiber tip of the PA source was incrementally translated through a cubic volume of 40x40x40 mm^3 . The center point of the cube was coincident with the point equidistant from all 15 transducers. The source was translated in 8 mm increments in the *x*, *y*, and *z*-directions providing a total of 216 test positions. At each test position, the PA signal was sampled for 10 laser pulses and averaged. The PA signal was recorded simultaneously on all 15 transducers and later analyzed to map signal amplitude, width, and time-of-flight for each position of the source in the imaging volume (see Fig. 1(c)).

3. Results

3.1 Source uniformity characterization

Figure 2 shows the results of the source uniformity characterization. Figure 2(a) illustrates the change in signal amplitude (peak-to-peak) as a function of the Intralipid percentage. For each combination of MB⁺ and IL, the average signal amplitude (represented by symbols) was computed using all 15 transducers. Error bars show the standard deviation computed over all three trials (45 total measurements). Each curve represents the result for a specific value of MB⁺ concentration. Figure 2(b) shows the coefficient of variation from the data corresponding to Fig. 2(a) as a function of Intralipid percentage. The coefficient of variation was found by

computing the ratio of the standard deviation to the mean value of each data point in Fig. 2(a). This indicated which of the PA sources statistically produced the most uniform signal. As was the case in Fig. 2(a), each curve represents a different methylene blue concentration.

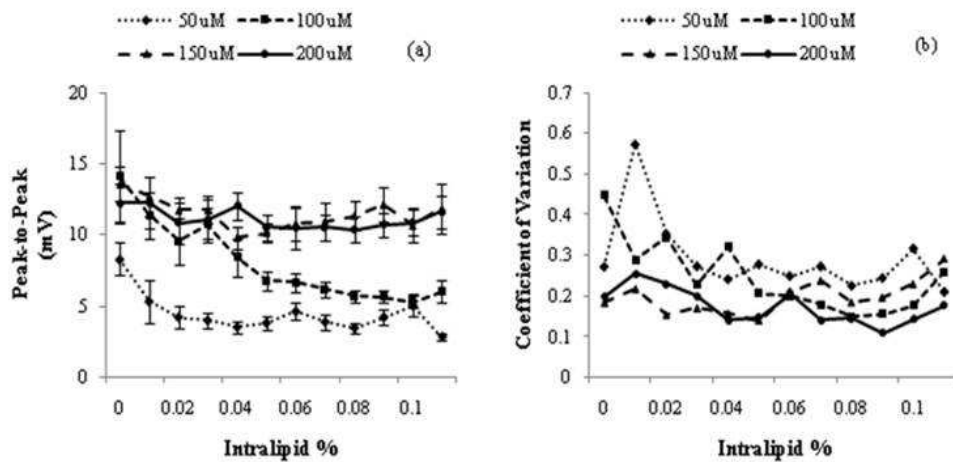


Fig. 2. (a) Peak-to-peak PA signal amplitude as a function of absorption (MB^+ , top legend) and scatter (Intralipid) for a liquid PA point source. Error bars represent \pm one standard deviation. (b) Coefficient of variation for data corresponding to (a).

3.2 Source directionality characterization

Figure 3 shows the results of the directionality characterization in both the zenith and azimuthal orientations of the $200 \mu\text{M MB}^+ / 0.09\%$ IL photoacoustic source. Each amplitude measurement was averaged over 5 laser pulses and subsequently averaged with each of the 3 experimental iterations. Error bars show the standard deviation for a given trial averaged over the 3 iterations. Each curve indicates a particular zenith elevation while each point on a curve indicates a distinct azimuthal position.

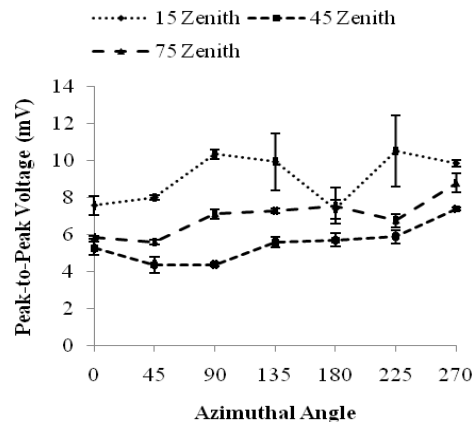


Fig. 3. Curves illustrating signal amplitude as a function of azimuthal position for varying zenith orientations. Error bars represent \pm one standard deviation.

3.3 System calibration scan

Figures. 4(a), 4(b), and 4(c) illustrate visually the characterization of signal amplitude, width, and time-of-flight, respectively, for each transducer at each position in the calibration volume. PA signals were analyzed as described in Fig. 1(c). Each column in Fig. 4 represents a particular transducer which corresponds to the transducer labeled in Fig. 4(i). Within a column, each of the 6 planar images illustrates an x-y plane at a different depth in the imaging volume.

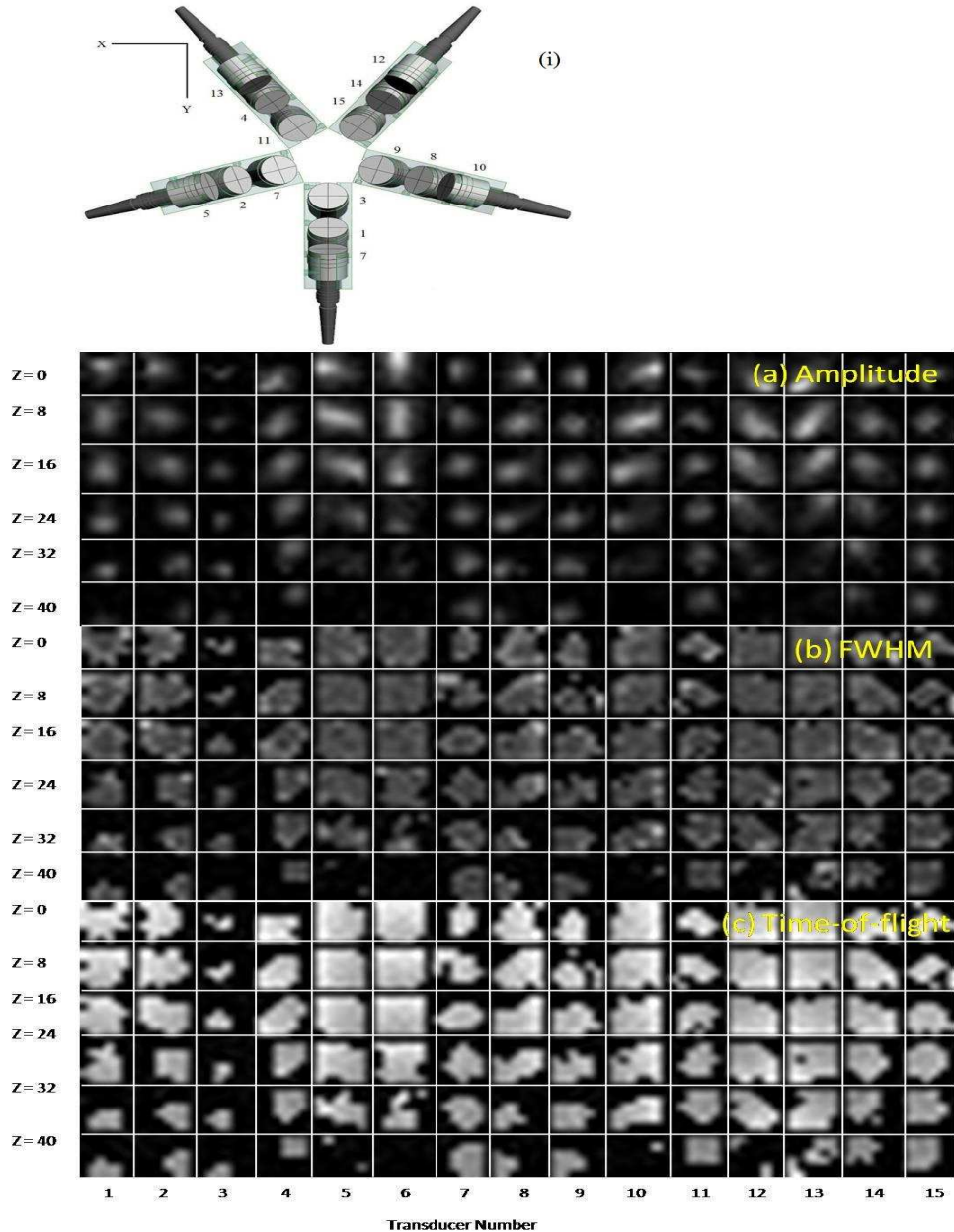


Fig. 4. Calibration maps of the metrics describing the PA signal detected by each transducer at each position within the calibration volume. (a) Signal amplitude - the magnitude of the peak-

to-peak voltage acquired (b) Signal width - the FWHM of the signal, and (c) Signal time-of-flight - a measure of the arrival time after laser trigger.

4. Discussion

4.1 Overview of basic finding

Photoacoustic imaging system characterization is important when directional sensitivity and/or the finite dimensions of acoustic transducers affect the detected PA signals. System characterization is essential if the variation in these properties differ among elements within the PA transducer array. The methodology developed and tested here promises to be useful for characterizing the system response of PA imaging systems, especially those that form an aperture with large solid angle. Furthermore, transducer-specific responses at multiple locations within the imaging volume provide information vital to the accurate reconstruction of photoacoustic images. The straightforward process of scanning an optical fiber within a reservoir of suitably designed liquid allows tuning of the resultant PA source and can be used to perform calibration scans tailored to PA transducer arrays that are optimized for a different spatial scales, e.g. $< 50 \mu\text{m}$ diameter fiber optic cable for a PA microscopy setup Vs. a larger diameter fiber for macroscopic ($\sim 1 \text{ mm}$) imaging setups. It is important to note that any attempt to scale a spherical source to the fiber diameter would need to accurately define important physical system parameters such as absorption coefficient, scattering coefficient, anisotropy in optical scatter, as well as the optical injection pattern (estimated by the fiber's numerical aperture). Modeling of the resulting optical distribution could then be estimated accurately by Monte Carlo simulations. In general, however, it is expected that the effective penetration depth of the light should be roughly half the diameter of the fiber to achieve an optical distribution that is approximately spherical. More specifically, the inverse of the total attenuation coefficient should be equal to half the diameter of optical fiber. This is of particular importance when tuning a PA source for systems beyond that used in this experiment.

4.2 MB^+/IL as a PA source

The motivation for the selection of the MB^+ concentration used to calibrate the transducer array was based on the observation that a plateau in signal strength was approached regardless of the concentration provided in the MB^+/IL solution. This trend is evident in Fig. 2(a) in which the MB^+/IL solutions of $150 \mu\text{M}$ and $200 \mu\text{M}$ provided PA signals with similar peak-to-peak signal amplitudes over much of the concentration range for Intralipid. It is intuitive to correlate signal amplitude with MB^+ concentration. The absorption coefficient of the liquid increases as the concentration of the MB^+ increases, resulting in larger peak-to-peak signal amplitudes. However, increasing the concentration of MB^+ will ultimately reduce the penetration depth of light into the liquid, reducing the effective dimensions of the source and the associated width of the PA signal. To conserve energy, the total area under the curve remains constant as the number of photons delivered to the system to create the acoustic signal is constant for each pulse. The transducers used in the experiments have a limited bandwidth. It is for this reason that the signal amplitude recorded by the transducers is not as straightforward as is determined by exclusively considering the absorption coefficient of the source. For a centre frequency of 2.25 MHz , the response peak occurs when an object is approximately $400\text{-}500 \mu\text{m}$. As the effective penetration depth of the source is decreased beyond these dimensions, the reduction in amplitude due to frequency response begins to compete with the increase in pressure wave amplitude due to the increased absorption. If the dimensions of the source were restricted further, eventually the transducer would not produce any signal as the frequency of the pressure wave would be outside the transducer's bandwidth. The selection of the optimal liquid was then made by comparing the coefficient of variation for each liquid combination. The coefficient of variation, shown in Fig. 2(b), permits selecting the MB^+/IL solution with the least signal variability among experimental iterations.

4.3 Variation in PA signal intensity as a function of zenith and azimuth

Although the initial characterization experiment to determine the optimal (i.e. lowest coefficient of variation) combination of absorption and scatter used the entire transducer array, the measurements were dependent on variations in sensitivity between transducers. This likely was present as a systematic error in the results presented in Fig. 2. To overcome this potential issue related to interpretation of the results, a PA source directionality characterization was completed with a single transducer mounted on a rotatable arm that permitted sensing of the PA signal from a variety of azimuthal and zenith positions at constant distance. This approach eliminated transducer-to-transducer variability as a contributing factor to signal fluctuations. We observed reasonable PA signal uniformity in the azimuthal direction and systematic decline in PA signal intensity as the zenith elevation angle increased. This was in contrast to our previously published work with a coated fiber-based PA source in which azimuthal signal uniformity was poor [13]. The decline in PA signal strength as a function of zenith, suggested that the light emitted from the fiber did not scatter and absorb as a perfect sphere. It is possible the fiber staining (described in 2.1) could have created a region of high MB⁺ concentration very close to the fiber tip. This would effectively create a gradient of MB⁺ concentration immediately below the surface of the fiber which could account for the zenith non-uniformity. Further detailed characterization of the liquid PA source with respect to the ratio of MB⁺/IL through experiment and perhaps Monte Carlo simulation might provide insight. The experimental results obtained with the liquid sources suggested that it may be better suited to transducer calibration procedures than coated optical fibers.

4.4 Calibration maps

The calibration maps shown in Fig. 4 visually illustrate the relative signal amplitude, width, and time-of-flight for many calibration locations within the imaging volume for every transducer. Figure 4(a), showing the signal amplitude at each calibration location, clearly indicates the directionality of each transducer. For example, transducer 12 and 13 (columns 12 and 13) stare at the imaging volume from an orientation off the acoustic axis. These results correlate well with the actual physical orientation of the transducers indicating the calibration map is accurately reporting signal sensitivity. Of interest is the extreme sensitivity reduction outside the axial line-of-sight for all transducers. This implied that signal generated and transmitted from a photoacoustic source off the acoustic axis (approximately ± 15 mm) could be easily concealed in the background noise. This suggests that the large 1" diameter transducers used to populate the transducer array confined the effective imaging volume to a spherical volume $30 \times 30 \times 30$ mm³ by the overlap of the calibration sensitivity maps. Figure 4(b) illustrates the behavior of the signal FWHM at each calibration location. The difference in FWHM is generally small from position to position. However, the outer edges of the imaging volume tend to broaden the acoustic signal as it sweeps over the face of the transducer as opposed to directly impinging the transducer when the signal propagates on the acoustic axis. While visibly difficult to discern, this trend is generally evident in the FWHM patterns in that they tend to show larger signals at the periphery of a given z-slice. As well, the complexity of the FWHM patterns indicates any modeling to predict the FWHM of a PA signal would be very difficult. Shown in Fig. 4(c) is the time-of-flight map. Perhaps the most important information garnered from the time-of-flight response is the presence of dark spots at a variety of locations in the imaging volume. Typically these positions were found in regions which corresponded to low signal amplitude (as seen in Fig. 4(a)). Likely, signals were masked in the noise and went undetected at those particular calibration positions because of the reduced amplitudes off the acoustic axis of a transducer.

4.5 Impact of calibration maps on image reconstruction

While the calibration scan did not specifically touch each voxel in the reconstructed imaging volume, the points absent from the scan were computed by linearly interpolating nearest neighbors. These values can be applied to the iterative reconstruction algorithm to modify the signal parameters attained when collecting image data. While this particular calibration scan has not been used to reconstruct new objects, previous scans have been applied to the reconstruction algorithm with success. The previous scans were implemented using sources of lower quality and still provided reasonable success [17].

4.6 Advantages/disadvantages of approach

In general, the liquid PA calibration source has proven to have a number of intrinsic advantages. Primarily, the inherent nature of the light propagation through a homogenous liquid is symmetric about the long axis of the optical fiber therefore leads to consistent PA signal emission in any azimuthal orientation. In comparison, manually constructed sources demonstrate azimuthal variability as a difficult obstacle to overcome as any physical imperfection in the source geometry translates to inconsistent acoustic sources. A second advantage of the liquid source is the ability for the user to tune the optical absorption and scatter coefficients very easily. This allows an experimenter the capability to affect the photoacoustic emission properties in a repeatable and simple manner. A significant shortcoming of the MB⁺/IL source was observed when the fiber optic was immediately placed within the liquid bath. Signal strength was initially much greater than the signal strength recorded after allowing the fiber to soak in the reservoir for approximately 20 minutes. Likely, this was observed due to MB⁺ staining of the fiber tip. While the experiments were always conducted after the soaking process, there was no certain length of time in which the signal would not reduce further. To that end, the signals produced were relatively small in magnitude compared to what might be considered ideal. The signal amplitude was adequate when the source was positioned directly on the acoustic axis but would more easily be masked by the background noise when off-axis as the signal-to-noise ratio was not as great as was seen in other omni-directional sources.

4.7 Future work

Improvements could be made on the photoacoustic source as well as the calibration process. Reasonably comprehensive experiments were conducted on a variety of different absorption and scattering combinations for the MB⁺/IL solution. The spherical-like shape of the source can be inferred from the signals detected by the hemispherical array of transducers. However, theoretical predictions attesting to the behavior of the source were not made. Monte Carlo simulations could be produced on light injected to a system of known scattering and absorption coefficients with known fiber specifications (numerical aperture and core diameter). As well, the current liquid solution seemingly stains the fiber optic after being immersed for a period of time. The liquid responsible for the absorption coefficient (in this case, methylene blue) could be replaced by a source with less significant staining or the fiber could be replaced by a fiber of different material, such as plastic. The calibration itself could be improved to provide enhanced coverage of the imaging volume. Specifically, the distance between successive steps in all planes could be reduced if the scanning system had the potential for greater speed. A calibration scan of 216 source positions takes approximately 1 hour to complete. Even doubling the number of calibration steps in each orientation (i.e. reducing step size from 8 mm to 4 mm) requires the calibration to have 1331 source positions if the imaging volume is maintained.

5. Conclusion

A liquid-based photoacoustic point source was developed and used to characterize signal amplitude, width, and time-of-flight for each voxel-transducer pair. The liquid source resulted in uniform signals via a liquid photoacoustic source in which scattering components provided the spherical light distribution in the liquid. A combination of MB⁺ at 200 μ M and IL at 0.09% proved to be the liquid solution with least variability in signal strength. Because the liquid source is inherently uniform in the azimuthal orientation, this source showed immediate improvement compared to previous iterations of an attempt to create an omni-directional photoacoustic source. Despite the promise seen in the signal consistency, the magnitude was typically much lower than that of previously used sources which allowed the signal to go undetected more rapidly. A calibration scan was completed with the liquid photoacoustic source in an imaging volume of 40x40x40 mm³ where signal amplitude, width, and time-of-flight were recorded. Ultimately, the source provided the photoacoustic system with supplementary information to be applied to the reconstruction algorithm in an effort to produce images of greater accuracy.

Acknowledgements

The authors would like to acknowledge Lynn Keenlside and John Patrick for their valuable technical help. Michael Roumeliotis is supported by the London Health Sciences Centre through the Translational Breast Cancer Research Unit (TBCRU) and by the University of Western Ontario (UWO). Pinhas Ephrat is supported by the Natural Sciences and Engineering Research Council (NSERC) and an Ontario Graduate Scholarship in Sciences and Technology (OGSST). Research funding was provided by the Ontario Research Fund (ORF), with the Canadian Found for Innovation (CFI), Natural Sciences and Engineering Research Council (NSERC), and MultiMagnetics Inc.